# Understanding of Light Absorption Properties of the N-Doped Graphene Oxide Quantum Dot with TD-DFT

Mohammed A. Jabed<sup>1</sup>, Julia Zhao<sup>1</sup>, Dmitri Kilin<sup>2</sup>, Tao Yu<sup>1\*</sup>

Corresponding author:

Tao Yu tao.yu.1@und.edu

<sup>&</sup>lt;sup>1.</sup> Department of Chemistry, University of North Dakota, Grand Forks, ND 58202

<sup>&</sup>lt;sup>2.</sup> Department of Chemistry, North Dakota State University, Fargo, ND 58105

### **Abstract**

We employed the TD-DFT method with different analyzing tools to systematically investigate the absorption properties of the C<sub>76</sub>H<sub>22</sub> and C<sub>73</sub>H<sub>21</sub> graphene quantum dots (GQD) with the oxygenous edge modification (oxidation with –OH and =O groups) and three types of the Ndoping defect. By analyzing the change of electronic structure, transition charge localization, noncarbon atomic orbital component, charge transfer magnitude, and transition dipole moment, we found the mechanisms of the oxygenous edge modification and N-doping in modulating absorption properties of the GQD materials relevant to the bioimaging application. Both the edge =O/-OH and the doped N can make a redshift for the absorption spectra. Only the =O group modification can turn the S<sub>1</sub> excitation to be a charge transfer state. The edge-modified =O and doped N alone is not sufficient to generate a strong intensity for the S<sub>1</sub> transition. Their combination can regulate the transition dipole moment distribution and enhance the intensity of S<sub>1</sub>. The edge-oxidation and N-doping induced electronic effects are also related to the deformation of the GQD planar structure. In particular, we developed a few analysis tools, including deformation maps and transition dipole moment maps, to virtualize the spatial resolution of the synergic effect of the heterogeneous atoms, O, OH, N, as well as the edge and core carbons. These results and analysis tools can provide more detailed information to understand the mechanisms of different types of edge modifications and defects at the atomistic level. They would be very useful for synthetic chemists to design novel quantum dots with a higher photoluminescence quantum yield.

### 1. Introduction

Graphene quantum dot (GQD) has promising functionalities in sensing applications,<sup>1</sup> bioimaging,<sup>2-4</sup> drug delivery,<sup>5</sup> and catalysis<sup>6</sup> due to its low toxicity,<sup>7</sup> water solubility,<sup>8</sup> biocompatibility<sup>9</sup>, and tunability of photophysical properties. One advantage of GQD lies in the fact that it can be easily synthesized at mild chemical conditions, and its properties can be easily tunable by chemical modifications and doping techniques. Despite GQD's open bandgap and promising optical properties, the realization of practical devices of GQD is challenging due to its edge effect (edge conformation or edge functionalization),<sup>10,11</sup> low quantum yield<sup>4</sup>, and lack of control on the photoluminescence mechanism<sup>8</sup>. It has been reported that the sp<sup>2</sup> network modification by doping,<sup>12,13</sup> edge modification,<sup>14</sup> and tuning defect side<sup>6,15</sup> could increase the quantum yield and change the photoluminescence (PL) energy. However, the exact mechanism is still under debate.

For GQD, two widely used techniques are employed to introduce various defects in the quantum dots, which can alter the GQD photoluminescence properties. One is to introduce heteroatoms or functional groups on the GQD edge, i. e. the boundary of GQD; and it is referred as edge modification. The other is to introduce heteroatoms or functional groups in the graphene honeycombed lattice (not the edge or boundary), and it is referred as doping. Regarding the edge modification, previous studies showed how alkylation increased the  $\pi$ -conjugation and increased the emission quantum yield for green-blue wavelength by minimizing the non-radiative recombination. 16 It was also reported that the blue PL in graphene quantum dots stems from the intrinsic  $\sigma$  to  $\pi^*$  transition, <sup>17,18</sup> and the green PL results from the edge defect states. <sup>17,19</sup> On the other hand, it was found that in graphene oxide quantum dots (GOQD), the blue emission arises from the radiative electron-hole recombination on the isolated sp<sup>2</sup> conjugated domains, which are separated by the sp<sup>3</sup> matrix.<sup>20</sup> Moreover, the origin of the green emission of GQD may stem from the generated localized state due to the charge transfer between spatially separated sp<sup>2</sup> and sp<sup>3</sup> dominated states.<sup>19</sup> Experimental and computational studies reported that the GQD edge effects have important roles in the induced PL phenomenon.<sup>2</sup> Meanwhile, chemical modifications by electron-donating groups like -OH<sup>2</sup> and electron-withdrawing groups, like -COOH, =O, are energetically favorable, 21-23 and would introduce a structural defect that can modulate the spatial localization of electron-hole as well as the emission energy. Meanwhile, these polarized edge groups enhance the GQD materials' solubility in the aqueous solution, which is crucial regarding

the bioimaging application. The hydroxide group functionalized graphene also has a pH-dependent photochemical feature.<sup>24</sup> Beyond that, studies have been demonstrated that these oxygenous groups influence the overall photophysics of the GQD by changing both electronic properties and structural deformation.<sup>25</sup>

Besides tuning the degree of sp<sup>3</sup>/sp<sup>2</sup> hybridized electron by chemical modification at edges or surfaces, the GQD's bandgap can be tuned by doping heteroatoms, including N<sup>15</sup>, B<sup>26</sup>, S, F<sup>27</sup>, P<sup>28</sup>, etc. N can be doped on the graphene in several conformations.<sup>29,30</sup> Replacing a carbon from the graphene's honeycomb motif with a nitrogen (we called it graphitic-N doping or simply N-doping) would move the Fermi energy toward unoccupied orbitals, which produces *n*-type doping effects.<sup>31</sup> Meanwhile, the doped nitrogen can also have the *p*-type doping effect when a pyridinic configuration is formed by C-C bond cleavage. The DFT studies show that the graphitic N could decrease the bandgap, and the induced charge transfer to the defected region would vary based on the type of N-doping.<sup>29</sup> Many applications have been reported using the N-doped GOQD materials, especially for oxygen reduction<sup>15,32</sup> and bioimaging.<sup>2</sup> The bioimaging application<sup>33,34</sup> requires strong PL quantum yield, strong capability for tissue penetration, and a long lifetime fluorescence signal. This drives many efforts to synthesize GOQD with red and near-infrared (NIR) emission properties. The N-doped graphene oxide quantum dot is one of the promising candidates regarding this purpose.<sup>10</sup>

Many theoretical investigations have been carried out to illustrate how the GOQD electronic structure was altered by the quantum confinement effect and the defect effect. 22,35 However, regarding the N-doped graphene oxide quantum dot (NGOQD) system, to our best knowledge, it is still a lack of a systematical study to understand and distinguish how the different types of defects, such as the edge modification with =O and –OH groups and various N-doping conformations, independently or synergistically modulate the optical properties of the GQD materials by examining the molecular orbital contribution, charge transfer feature, localized transition dipole moment, and structural deformation.

In this particular work, we focus on investigating the absorption properties of the oxygenous edge-modified graphene and nitrogen-doped graphene quantum dots using the linear-response time-dependent density functional theory (TD-DFT).<sup>20,36</sup> This work aims to understand the molecular mechanisms of different chemical factors modulating the absorption properties of

GQD, which can provide many useful physical insights to design GQD-based nanomaterials with a high PL quantum yield in the NIR wavelength range for the bioimaging application. To this end, we employed the strategy of variable control and performed systematical studies by separately investigating the effect induced by the edge modification with =O and –OH groups and the effect induced by doping three different types of N in the lattice of GQD. Our work not only focuses on analyzing the localized effect induced by the modifications and defects, i.e., perturbing the local binding environment; but also concentrates on understanding the consequence regarding the change of the electron density within the overall graphene structure, such as the charge transfer feature, transition dipole moment, and the modification/defect-induced deformation of the graphene planar structure, which may lead to a symmetry-breaking; therefore, significantly tuning the electronic properties of the GQD materials.

## 2. Computational Methodologies

Two GQD models were employed in this work. C<sub>76</sub>H<sub>22</sub> is used to build the edge modified structure with caping =O or –OH groups, and C<sub>73</sub>H<sub>21</sub> is used to construct the N-doped structures. The odd number of H atoms in the latter case made a closed-shell structure after doping one N-atom. For studying the effects of oxygenous edge modification, the =O and –OH groups were substituted on the edge of the graphene quantum dot, C<sub>76</sub>H<sub>22</sub> to generate the modeling graphene oxide (GO) and graphene hydroxide (GOH) quantum dots. In particular, we focused on four model structures by introducing 10 and 22 =O and –OH, named GO10, GOH10, GO22, and GOH22 (**Figure 1**). For GO10 and GOH10, the oxygenous groups were added in the same positions where the =O and –OH were evenly distributed along the edge of the quantum dot. On the other hand, the N-doping effect was investigated using three structures representing three different doping types, labeled as GNa, GNb, and GNc, as shown in **Figure 1**. Models of N-doped graphene oxide quantum dots (NGOQD) with varying numbers (4, 6, 8, 10, and 20) of =O groups on edge were also investigated (**Figure S1**).

All geometries were optimized using the density functional theory (DFT)<sup>37</sup>, and excited state energies were calculated using the linear response time-dependent DFT (TD-DFT).<sup>38</sup> The hybrid exchange-correlation functional, Perdew-Burke-Ernzerhof (PBE0)<sup>39</sup> was employed in this work. The previous benchmark calculation showed that the calculated excitation energy of the

graphene system using the PBE0 functional with the 6-31G\* basis set<sup>40</sup> had good agreement with the experiment measurement.<sup>41</sup> Meanwhile, the PBE0 functional predicted an adequate description of the electronic properties of the extended systems like graphene.<sup>42-45</sup> All the ground state and excited state calculations were performed with the solvation effect using the conductor like polarizable continuum model (CPCM).<sup>46</sup> The absorption spectra were obtained by Gaussian broadening of the excited state energies with 0.08 eV thermal broadening. Several studies suggested that 0.08 eV broadening would show an acceptable spectral feature of the similar extended  $\pi$ -conjugated system.<sup>47</sup> All the DFT and TD-DFT calculations were performed in the Gaussian16 software packages<sup>48</sup>, and all charge density distribution images were visualized using VMD code.<sup>49</sup>

The charge transfer (CT) character of a system was obtained by computing the charge transfer length ( $\Delta r$ ).<sup>50</sup> With the virtual and occupied molecular orbitals in each excitation state, the charge transfer length ( $\Delta r$ ) represents the electron-hole distance in each excitation evaluated with

$$\Delta r = \frac{\sum_{mn} K_{mn}^2 \left| \langle \varphi_n | r | \varphi_n \rangle - \langle \varphi_m | r | \varphi_m \rangle \right|}{\sum_{mn} K_{mn}^2} \tag{1}$$

where  $\varphi_m$ ,  $\varphi_n$  are the occupied and unoccupied molecular orbitals, and r is the position.  $K_{mn}$  is the transition coefficient of a single electron excitation calculated using the TD-DFT method.

In the case of  $\pi$ -conjugated organic aromatic, it was reported that a ground state transition of  $\Delta r > 2.0$  can be considered as CT type transition<sup>50,51</sup>. Graphene and graphene oxide QDs have a higher density of the  $\pi$ -electron network as such  $\Delta r$  is a good qualitative descriptor for the CT nature of a transition. The structural deformation of the graphene and its derivatives were characterized by the norm of each atom on a defined plane. Detailed methodology of the distortion plot is given in the supporting information.

### 3. Result and Discussion

The defects on the edge and interior lattice range of GQD can provide a comprehensive and synergic mechanism that affects the optical properties of the materials. In this work, to better illustrate the roles of the edge and lattice defects, we control structural variables by considering the edge oxygenous effect and the N-doping effect in a separate fashion, and then we combine

these two effects and investigate the target NGOQD materials. We focus on the defect-induced change of (a) geometry structure, (b) spectrum feature (peak position and intensity), (c) molecular orbital component and electron/hole density feature, (d) charge-transfer character, and (e) transition dipole moment in each analysis; and seek for their correlation to understand the mechanism of the defect-tuning absorption properties in chemistry language. Here the bullet points are highlighted. One, both the oxygenous edge modification and N-doping can make the absorption spectra redshifted due to the mixing of the oxygen and nitrogen atomic orbitals with graphene-carbon molecular orbitals. Two, the electron withdrawing =O groups on edge can localize the charge transition and enhance the charge transfer character in excited states. Three, the role of the doped N atom depends on its binding environment with the carbon lattice. Four, the edge =O and doped N alone is insufficient to generate a strong intensity for the  $S_1$  transition. Their combination can regulate the transition dipole moment and enhance the  $S_1$  absorption intensity. Five, we noticed that the electronic effect, including the change of transition charge localization, non-carbon atomic orbital component, the charge transfer magnitude, and the transition dipole intensity, are related to the deformation of the GQD planar structure induced by the edge and lattice defects.

## 3.1 The oxygenous edge modification effect

To vary the edge effect, we investigated four oxygenous modified GQD with different O/C ratios. They are named GOH10, GO10, GOH22, and GO22, and their optimized structures are displayed in **Figure 1e-h**. **Figure 2a** shows their linear optical absorption spectra in an excitation-energy window lower than 3.00 eV. The absorption spectrum of pristine graphene (G) can be considered as a reference. It shows two distinctive and relatively narrow absorption peaks due to the confinement effect, dominated mainly by the S<sub>1</sub> and S<sub>5</sub> excitation. Compared with the reference spectrum of pristine graphene, GOH10, GOH22, GO10, and GO22 display a significant redshift for the overall absorption pattern (**Figure 2a**), which agrees with experimental studies.<sup>20</sup> Meanwhile, we noticed that (1) the =O modification could cause a larger redshift than –OH, and (2) a larger redshift can be obtained by introducing more edge =O or –OH groups. For instance, in the S<sub>1</sub> excitation, the peaks are redshifted to 1.70 eV, 1,62 eV, 0.27 eV, 0.18 eV for GOH10, GOH22, GO10, and GO22, respectively. This indicates that GO10 and GO22 can be considered promising candidates for the NIR bioimaging applications; however, their oscillator strengths are

very weak (the oscillator strength is 0.004 and 0.0002), as shown in **Table 1**. More engineering effort is needed to improve their absorption intensities.

Here, we focus on analyzing the mechanism of the edge –OH and =O induced redshift. The molecular orbital (MO) component analysis demonstrates that the =O modification has a greater oxygen atomic orbital (AO) contribution than the –OH modification (Table 1). When the graphene edge is capped with more oxygenous groups, the oxygen AO contribution is increased. The mixture of oxygen AO significantly alters the energy levels, and the related MO energy diagrams can be found in Figure S2. In addition, the charge density difference maps (the electron density difference between the ground state and excited state) are shown in Figure 3, which provides a visualization tool to analyze the change of electron distribution in excited states. For G (Figure 3a), the two excitations ( $S_1$  and  $S_5$ ) have the alternating positive and negative charge density difference along with the conjugated C-C bonds. This result mainly stems from the HOMO-to-LUMO  $(\pi$ -to- $\pi$ \*) transitions in the pristine graphene. Meanwhile, it is found that the -OH modification did not significantly alter the graphene charge density difference map (Figure 3d, e). In particular, little charge density difference distribution was found localized on the –OH groups. Therefore, this result indicates that the oxygenous sp<sup>3</sup> effect in the -OH groups do not alter the transition character; and it is still the  $\pi$ -to- $\pi$ \* MO transitions in the GOH10 and GOH22 quantum dots. That is why their absorption patterns are very similar to the reference (G) with a small redshift (Figure 2a). By contrast, for both GO10 and GO22, a significant charge density difference contribution localized on the edge =O groups (Figure 3b, c), which demonstrates a different mechanism that the oxygenous orbitals, the nonbonding lone-pair 2p orbitals and the bonding sp<sup>2</sup> orbitals play significant roles in tuning the excitation transitions. As a result, more complicated MO transition pairs are recognized beyond the  $\pi$ -to- $\pi$ \* transition. This result is consistent with the observation that the absorption patterns of GO10 and GO22 are different from the reference graphene (G) (Figure 2a).

Furthermore, we notice that the electron-donating –OH and electron-withdrawing =O groups can generate different intramolecular charge transfer characters in excited states, which is important for understanding the PL properties. The charge transfer (CT) in GQD can be used to quench the fluorescence signal generated by other organic dye molecules.<sup>52</sup> On the other hand, the direct recombination of the spatially separated charges in the CT state can generate fluorescence

for the GQD PL applications.<sup>53</sup> Therefore, it is necessary to investigate the CT character quantitively and understand how it is impacted by the oxygenous edge modification. To this end, we calculated the charge transfer length (CTL,  $\Delta r$ ) using eq. 1 for the target quantum dots (**Table 1**). For instance, in S<sub>1</sub>, it is found that (1) the =O modification has a larger CTL than the –OH modification, and (2) CTL is increasing with increasing the number of oxygenous groups. Based on the literature studies, wherein the case of conjugated organic compounds, a dominated charge transfer state can be defined by CTL greater than 2.0 Å when calculated using the GGA functional or greater than 3.0 Å when calculated using the hybrid GGA functional.<sup>50</sup> We conclude that the S<sub>1</sub> in GO10 and GO22 is a charge transfer state, which indicates that the =O groups can stabilize the photoinduced charge separation.

Besides, we notice that the effect of edge oxygenous modifications is not only originated from the electronic effect of =O and –OH, but also related to the carbon-lattice structural changes caused by the oxidations. Unlike a large-scale graphene sheet, GQD has a flat planar structure due to the sp² hybridization of all carbons. After the oxygenous edge modifications, a significant structural deformation was observed for both the GOH and GO quantum dots, as shown in **Figure 1e-h**. This deformation reduces the QD's symmetry and interrupts the conjugated carbon network. As a result, the delocalization character of molecular orbitals can be attenuated, leading to more localized electrons and holes in the charge density difference maps and a larger CTL in the absorption process. Also, the previous studies have been demonstrated that the sp² interruption and the localizations play a significant role in the PL process. <sup>18,20</sup>

To quantitatively characterize the deformation effect, we analyzed the distribution of the out-of-plane carbon atoms for the GOH and GO quantum dots. As shown in **Figure 4a**, **b**, **d**, **e**, the spatially resolved color-coded deformation maps were used to demonstrate how the carbon atoms were deformed by the edge oxygenous modifications. For both the GOH and GO quantum dots, it is found that the deformation mainly occurred near the QD edge range. The corresponding histograms (**Figure 4c**, **f**) suggest that the higher O/C ratio results in a larger deformation. In addition, GO has a larger deformation than GOH. The average edge C-C bond length is 1.39 Å in GQD, which agrees with the characteristic bond length of the sp<sup>2</sup> hybridization. Similarly, the average edge C-C bond lengths are 1.39 Å and 1.40 Å GOH10 and GOH22, respectively, very close to GQD. In contrast, the average edge C-C bond length increases to 1.41 Å and 1.45 Å in

GO10 and GO22, respectively. A longer bond length indicates a more interruption of the sp<sup>2</sup> conjugation. This result is consistent with the previous discussion, which shows the –OH groups slightly perturb the electronic structure of GQD, but the =O groups introduce a significant electronic structure change.

## 3.2 The N-doping effect

Nitrogen doping in graphene was reported as a very efficient method to increase the optoelectronic and sensing properties of the graphene QD.<sup>15,29</sup> There are many different N-doping types,<sup>29</sup> and we consider three of them in this work, which has the nitrogen binding in the graphene lattice with different binding environments, as shown in **Figure 1b**, **c**, **d**. The first one, labeled as GNa, is doping an N atom by replacing a non-edge C atom but preserving the three covalent bonds with the nearby carbons. It would allow an excess electron from N delocalized to the graphene lattice and can be recognized as an *n*-type doping effect, which is also known as the graphitic N doping.<sup>29,31</sup> The second type, labeled as GNb, is a pyridinic type doping with the doped N connected with two carbons, which breaks the conjugated network of the graphene lattice. It shifts the Fermi level close to the unoccupied band, which creates a *p*-type doing effect.<sup>29,31,54,55</sup> The third one, labeled as GNc, is doping an N atom as covalently adsorbed on the graphene plane, where the N atom bond with two C atoms.

In experiments, different N-doping rates or N/C ratios can be achieved from 1% to 7%. 6,10 We concentrated on a single doped N atom, and the N/C ratio is about 1.4% in this work. The higher doping rate with multiple doped N atoms can be very complicated by considering a combination of doping types and various doping positions. We focus on the quantum dots with one doped N atom in the graphene center, which can provide a clear picture to understand the fundamental roles of N in the optical properties. **Figure 2b** shows the absorption spectra of the three different N-doped graphene (GN) quantum dots. They show significantly red-shifted absorption spectra, but the overall spectral features are still consistent with the reference absorption spectrum of the corresponding pristine graphene quantum dot. This redshift observation is consistent with the experimental studies, 10 and it suggests that the N-doping has a similar effect as the –OH edge modification as discussed in **section 3.1**. However, their mechanisms are different. Unlike GOH, where the –OH groups perturb the carbon MO from the edge, these three GN

quantum dots interrupt the bonding environment of the carbon network in the center of the plane, resulting in a significant change of the GQD electronic structure. The corresponding MO energy diagrams are shown in **Figure S2**. In **Table 1**, it is shown that the first excited state energy in all three cases is less than 1.00 eV. However, they are optically dark transitions, and the absorption peak intensity is close to zero. The three bright peaks in the range of 1.50-3.5 eV are from higher excitation levels.

Even though the S<sub>1</sub> transitions in the three N-doped GQD has negligible oscillator strength, it is still worthwhile studying their properties, which would provide physical insights to understand the N-doping effect and develop a new doping strategy to enhance the absorption intensity. By the orbital component analysis for the S<sub>1</sub> transition (**Table 1**), it is noticed that GNa only has the nitrogen AO contribution in the unoccupied MO. GNb and GNc include the nitrogen AO contribution for both the occupied and unoccupied MO, and the contribution in the occupied MO is higher than unoccupied MO.

To further investigate the N-doping electronic effect, the electron charge density difference maps were analyzed to discuss the electron density redistribution associated with excitations. As shown in **Figure 5-a**, **g**, **h**, it is noticed that the charge density difference can be found on the doped nitrogen atoms. In particular, for GNa, the N atom has an extra electron density indicating it acts as an electron acceptor at the excited states. By contrast, for GNb and GNc, the N atom has a hole density which indicates it performs as an electron donor in the excited states. Meanwhile, GNc has a greater hole density than GNb, and this can be because the two N-C bonds and the lone-pair electrons from the out-of-plane N atom in GNc can have a larger impact on the C-C  $\pi$  bond.

Another essential aspect regarding the N-doping induced electronic effect is to study the charge transfer character for each case (**Table 1**). First, we noticed that GNa has a smaller CTL than GNb and GNc, consistent with the charge density difference map analysis. In general, a delocalized charge density difference map has a smaller CTL, and a localized charge density difference map can have a larger CTL. For instance, for S<sub>1</sub>, the GNc has a strong electronic localization at the defect N atom, the largest CTL, 1.87 Å was found among the three quantum dots. Second, we notice that the calculation of CTL values for the excited states are all less than 2.0. Therefore, we conclude that, unlike the edge =O group modification, the N-doping cannot generate a charge transfer predominated state. The reason can be (1) the N atom has less electron

negativity than the O atom, (2) only one N atom was doped, but multiple O atoms were modified in our study, and (3) the oxygenous edge modification creates a structural change in a higher degree than N.

The observed structural deformation also echoes this structural change induced by the N-doping. It is found that the three doping types have different impacts on the graphene planar structure. The corresponding deformation map is displayed in **Figure 6**. Note that the GNa and GNb slightly deform the graphene structure. Therefore, the nearby carbon-carbon conjugated network is slightly interrupted. Instead, the GNc can not only directly pull out the two connected carbon atoms but also affect their neighbors and cause a significant localized deformation in the planar structure (**Figure 1d**). This feature in GNc is another essential reason for its strong charge density difference localization and forming a hole trap.

## 3.3 N-doped graphene oxide

The discussion above demonstrates that the N-doped GQD can modulate the electronic structure of the quantum dot and can induce lower energy absorptions. However, they do not have good aqueous solubility, and the absorption intensities for the fluorescence relevant  $S_1$  excitation is optically dark. Therefore, strategies are required to remove these two barriers for their applications in bioimaging. One solution is to integrate the oxygenous edge modification with the N-doping. The previous study indicated that introducing electronegative =O groups would change the N-doping GQD electric dipole, creating an optically active state. <sup>56</sup> In this section, we focus on the GNa quantum dot with the =O group edge modification to understand the synergic effects from the graphene-lattice doping defect and the edge functionalization. In particular, we focus on investigating the chemical reason why the combination of these two defects can enhance the  $S_1$  absorption intensity. The studies integrating the GNb and GNc with the edge modification will be carried out in our future work.

First, to find the optimized O/C ratio for GNa, which produces the brightest S<sub>1</sub> absorption, we constructed several GNa quantum dots with 4, 6, 8, 10, and 20 edge =O groups, name GNaO4, GNaO6, GNaO8, GNaO10, GNaO20, respectively. Their optimized geometries (**Figure S1**) suggest that they slightly deform the planar structure except GNaO20 (**Figure S3**). Their absorption spectra are shown in **Figure 2c**, **d**. The results demonstrate that the edge oxidation

raises three essential effects. First, the absorption peaks are further redshifted compared with GNa. Second, the charge density difference maps (**Figure 5b-f**) indicate that the oxidation initializes more charge localization in  $S_1$ . Consequently, their  $S_1$  states have a much larger CTL than GNa, and the  $S_1$  can be identified as charge transfer states (**Table 1**). Third, it is noticed that with smaller O/C ratios, such as GNaO4 and GNaO6, the edge oxidation enhances the  $S_1$  oscillator strength significantly (**Table 1**). Our studies demonstrate the versatile effects of the edge =O groups in GNa in terms of tuning the electronic structure, enhancing the charge localization and charge transfer feature, as well as enhancing the transition dipole moment for the  $S_1$  excitation, which potentially increase the quantum yield of fluorescence emission within the NIR range.

To illustrate the mechanism of the integration of the edge =O modification and center N defect in regulating the intensity of the S<sub>1</sub> excitation, we decomposed the transition dipole moment into the contribution from the carbon, nitrogen, and oxygen atoms using the Multiwfn code<sup>57</sup> (Table 2). Figure 7 is showing the spatially resolved transition dipole moment (TDM) contribution of individual atoms. First, the transition dipole moment is predominated by the Xcomponent and predominately contributed by the edge carbons in the graphene quantum dot. For GO22, the TDM contribution can be found on the oxygens as well as the core and edge carbons in all directions. Even the overall effect is a significant cancellation, the existence of the 22 edge oxygens induces a redistribution of TDM among the edge and core carbons in all directions, compared with the G reference. On the other hand, the GNa creates a defect in the center of the graphene sheet. However, it shows that almost no TDM can be found on the N defect site. Instead, the TMD's of its secondary bonding carbons are significantly enhanced (Figure 7c). Furthermore, this effect can propagate onto the edge carbons, especially along the X- and Y-directions. A similar result is observed in GNb (Figure S5). However, GNc shows a different pattern in the TDM map. It shows that its TDM is localized on the out-plane N defect (Figure S6), and smaller contributions can be found on carbons. This result is consistent with the discussion in section 3.2, which demonstrated a very localized hole-trap character on the defect site. Note that although both the 22 edge =O groups and center GNa defect can induce atomic TDM cancellation (Figure 7b, c), they have different molecular mechanisms. Interestingly, when combining the N defect with the edge oxidation, the N's impact on the nearby carbon is reduced (Figure 7d, e, Figure S7-S9), and larger TDM's can be found on the edge carbons and oxygens (Table 2). Although high O/C ratios (GNaO20) can achieve small intensity improvement with respect to GNa, the edge oxidation with

the four =O groups converts the GNa's dark  $S_1$  excitation state to a bright one. Similar results are observed by the edge oxidation with 6, 8, and 10 =O groups. This trend can be related to the observation that the higher O/C ratio case, GNaO20 induces a significantly larger deformation effect compared with the other cases with a lower O/C ratio (**Figure S3**).

### 4. Conclusion

In this work, we employed the TD-DFT method together with several analyzing tools to investigate both the edge oxygenous modification effect and the N-doping effect on regulating the optical absorption properties of graphene quantum dot materials. Our studies did not aim to investigate and screen all the possible influences of multiple structural factors, such as modification and doping site variation, doping rate variation, doping position variation, etc. Instead, we concentrated on the representative cases reported in the literature and identified general trends. Specifically, to "virtualize" the change of the electronic structures and the perturbation of the graphene lattice geometry induced by the edge-modification and N-doping, we highlighted the charge density difference map, deformation map, and transition dipole moment map to obtain the spatially-resolved information and mechanism regarding the absorption process in the modeled quantum dots. It is found that the O or N induced deformation makes the GQD planar symmetry broken, which not only diversifies the electronic structure and interrupts the conjugated carbon network, but also opens more orbital transition channels in the photoexcitation. Exploration of this trend did allow us to identify specific structure-to-property relations. Meanwhile, we noticed that the transition charge localization, non-carbon atomic orbital component, charge transfer magnitude, and transition dipole magnitude are all related to the change of the quantum dot's structure by the edge ligands modification and doping. The main practical findings of this work identify individual and synergistic effects of O and N atoms as follows:

- (1) both the edge oxygenous modification and N-doping can make a redshift for the quantum dot's absorption spectra,
- (2) the edge-modified =O groups can stabilize the localized charge transition and can turn the S<sub>1</sub> excitation to be a charge transfer state, and

(3) the edge-modified =O or center-doped N alone is not sufficient to generate a strong intensity for the  $S_1$  transition, and their combination can regulate the transition dipole moment and enhance the intensity of the  $S_1$  transition.

To summarize, we conclude that using the graphitic N-doping with a lower-O/C-ratio edge oxygenous modification, the quantum dots can have the best redshift and bright S<sub>1</sub> excited states. We believe that the reported findings may impact both computational and experimental research communities. Specifically, the use of deformation, charge density difference, and transition dipole moment maps can provide detailed information to understand the mechanism of other types of defects and modifications. To our best knowledge, it is not easy to achieve a precise control of the O/C and N/C ratio during the synthesis, and a mixture of N-doped graphene quantum dots is usually obtained. Our study would be very useful to encourage synthetic chemists to develop more advanced synthetic and separation techniques to design novel graphene quantum dots with a higher photoluminescence quantum yield.

## Acknowledgments

The authors acknowledge the support of the startup fund from the University of North Dakota. This work used high-performance computing resources provided by the University of North Dakota Computational Research Center and the Center for Computationally Assisted Science and Technology (CCAST) at North Dakota State University. Also, this work was supported, in part, at the Center for Integrated Nanotechnologies, an Office of Science User Facility operated for the U.S. Department of Energy (DOE) Office of Science by Los Alamos National Laboratory (Contract 89233218CNA000001) and Sandia National Laboratories (Contract DE-NA-0003525) along user allocation 2019BU0186: "Magnetic and Nonadiabatic Driven Dynamics in 2D Materials". This work was partially supported by the NSF grant CHE 1709160.

# **Supporting information**

The supporting information provides the methodology of deformation maps, orbital energy diagrams, the top and side view of the structure of GNaO4, GNaO6, GNaO8, and their deformation and transition dipole moment maps.

## **Reference:**

- (1) Wu, X.; Tian, F.; Wang, W.; Chen, J.; Wu, M.; Zhao, J. X. Fabrication of highly fluorescent graphene quantum dots using l-glutamic acid for in vitro/in vivo imaging and sensing. *J. Mater. Chem. C* **2013**, *1*, 4676-4684.
- (2) Zhu, S.; Zhang, J.; Qiao, C.; Tang, S.; Li, Y.; Yuan, W.; Li, B.; Tian, L.; Liu, F.; Hu, R.; Gao, H.; Wei, H.; Zhang, H.; Sun, H.; Yang, B. Strongly green-photoluminescent graphene quantum dots for bioimaging applications. *Chem. Commun.* **2011**, *47*, 6858-6860.
- (3) Schroer, Z. S.; Wu, Y.; Xing, Y.; Wu, X.; Liu, X.; Wang, X.; Pino, O. G.; Zhou, C.; Combs, C.; Pu, Q.; Wu, M.; Zhao, J. X.; Chen, J. Nitrogen–Sulfur-Doped Graphene Quantum Dots with Metal Ion-Resistance for Bioimaging. *ACS Appl. Nano Mater.* **2019**, *2*, 6858-6865.
- (4) Li, L.; Wu, G.; Yang, G.; Peng, J.; Zhao, J.; Zhu, J.-J. Focusing on luminescent graphene quantum dots: current status and future perspectives. *Nanoscale* **2013**, *5*, 4015-4039.
- (5) Wang, X.; Sun, X.; Lao, J.; He, H.; Cheng, T.; Wang, M.; Wang, S.; Huang, F. Multifunctional graphene quantum dots for simultaneous targeted cellular imaging and drug delivery. *Colloids Surf. B. Biointerfaces* **2014**, *122*, 638-644.
- (6) Dumont, J. H.; Martinez, U.; Artyushkova, K.; Purdy, G. M.; Dattelbaum, A. M.; Zelenay, P.; Mohite, A.; Atanassov, P.; Gupta, G. Nitrogen-Doped Graphene Oxide Electrocatalysts for the Oxygen Reduction Reaction. *ACS Appl. Nano Mater.* **2019**, *2*, 1675-1682.
- (7) Baker, S. N.; Baker, G. A. Luminescent Carbon Nanodots: Emergent Nanolights. *Angew. Chem. Int. Ed.* **2010**, *49*, 6726-6744.
- (8) Zhu, S.; Zhang, J.; Liu, X.; Li, B.; Wang, X.; Tang, S.; Meng, Q.; Li, Y.; Shi, C.; Hu, R.; Yang, B. Graphene quantum dots with controllable surface oxidation, tunable fluorescence and up-conversion emission. *RSC Adv.* **2012**, *2*, 2717-2720.
- (9) Peng, J.; Gao, W.; Gupta, B. K.; Liu, Z.; Romero-Aburto, R.; Ge, L.; Song, L.; Alemany, L. B.; Zhan, X.; Gao, G.; Vithayathil, S. A.; Kaipparettu, B. A.; Marti, A. A.; Hayashi, T.; Zhu, J.-J.; Ajayan, P. M. Graphene Quantum Dots Derived from Carbon Fibers. *Nano Lett.* **2012**, *12*, 844-849.
- (10) Das, S. K.; Luk, C. M.; Martin, W. E.; Tang, L.; Kim, D. Y.; Lau, S. P.; Richards, C. I. Size and Dopant Dependent Single Particle Fluorescence Properties of Graphene Quantum Dots. *J. Phys. Chem. C* **2015**, *119*, 17988-17994.
- (11) Tang, L.; Ji, R.; Li, X.; Teng, K. S.; Lau, S. P. Size-Dependent Structural and Optical Characteristics of Glucose-Derived Graphene Quantum Dots. *Part. Part. Syst. Charact.* **2013**, *30*, 523-531.
- (12) Haberer, D.; Giusca, C. E.; Wang, Y.; Sachdev, H.; Fedorov, A. V.; Farjam, M.; Jafari, S. A.; Vyalikh, D. V.; Usachov, D.; Liu, X.; Treske, U.; Grobosch, M.; Vilkov, O.; Adamchuk, V. K.; Irle, S.; Silva, S. R. P.; Knupfer, M.; Büchner, B.; Grüneis, A. Evidence for a New Two-Dimensional C4H-Type Polymer Based on Hydrogenated Graphene. *Adv. Mater.* **2011**, *23*, 4497-4503.
- (13) Haberer, D.; Vyalikh, D. V.; Taioli, S.; Dora, B.; Farjam, M.; Fink, J.; Marchenko, D.; Pichler, T.; Ziegler, K.; Simonucci, S.; Dresselhaus, M. S.; Knupfer, M.; Büchner, B.; Grüneis, A. Tunable Band Gap in Hydrogenated Quasi-Free-Standing Graphene. *Nano Lett.* **2010**, *10*, 3360-3366.
- (14) Tachi, S.; Morita, H.; Takahashi, M.; Okabayashi, Y.; Hosokai, T.; Sugai, T.; Kuwahara, S. Quantum Yield Enhancement in Graphene Quantum Dots via Esterification with Benzyl Alcohol. *Sci. Rep.* **2019**, *9*, 14115.
- (15) Zhang, Y.; Ge, J.; Wang, L.; Wang, D.; Ding, F.; Tao, X.; Chen, W. Manageable N-doped Graphene for High Performance Oxygen Reduction Reaction. *Sci. Rep.* **2013**, *3*, 2771.
- (16) Zhu, S.; Zhang, J.; Tang, S.; Qiao, C.; Wang, L.; Wang, H.; Liu, X.; Li, B.; Li, Y.; Yu, W.; Wang, X.; Sun, H.; Yang, B. Surface Chemistry Routes to Modulate the Photoluminescence of Graphene

Quantum Dots: From Fluorescence Mechanism to Up-Conversion Bioimaging Applications. *Adv. Funct. Mater.* **2012**, *22*, 4732-4740.

- (17) Pan, D.; Zhang, J.; Li, Z.; Wu, M. Hydrothermal Route for Cutting Graphene Sheets into Blue-Luminescent Graphene Quantum Dots. *Adv. Mater.* **2010**, *22*, 734-738.
- (18) Heitz, T.; Godet, C.; Bourée, J. E.; Drévillon, B.; Conde, J. P. Radiative and nonradiative recombination in polymerlike a–C:H films. *Phys. Rev. B.* **1999**, *60*, 6045-6052.
- (19) Wang, L.; Zhu, S.-J.; Wang, H.-Y.; Qu, S.-N.; Zhang, Y.-L.; Zhang, J.-H.; Chen, Q.-D.; Xu, H.-L.; Han, W.; Yang, B.; Sun, H.-B. Common Origin of Green Luminescence in Carbon Nanodots and Graphene Quantum Dots. *ACS Nano* **2014**, *8*, 2541-2547.
- (20) Eda, G.; Lin, Y.-Y.; Mattevi, C.; Yamaguchi, H.; Chen, H.-A.; Chen, I.-S.; Chen, C.-W.; Chhowalla, M. Blue Photoluminescence from Chemically Derived Graphene Oxide. *Adv. Mater.* **2010**, *22*, 505-509.
- (21) Page, A. J.; Chou, C.-P.; Pham, B. Q.; Witek, H. A.; Irle, S.; Morokuma, K. Quantum chemical investigation of epoxide and ether groups in graphene oxide and their vibrational spectra. *Phys. Chem. Chem. Phys.* **2013**, *15*, 3725-3735.
- (22) Chen, S.; Ullah, N.; Wang, T.; Zhang, R. Tuning the optical properties of graphene quantum dots by selective oxidation: a theoretical perspective. *J. Mater. Chem. C* **2018**, *6*, 6875-6883.
- (23) Chua, C. K.; Sofer, Z.; Šimek, P.; Jankovský, O.; Klímová, K.; Bakardjieva, S.; Hrdličková Kučková, Š.; Pumera, M. Synthesis of Strongly Fluorescent Graphene Quantum Dots by Cage-Opening Buckminsterfullerene. *ACS Nano* **2015**, *9*, 2548-2555.
- (24) Pan, D.; Zhang, J.; Li, Z.; Wu, C.; Yan, X.; Wu, M. Observation of pH-, solvent-, spin-, and excitation-dependent blue photoluminescence from carbon nanoparticles. *Chem. Commun.* **2010**, *46*, 3681-3683.
- (25) Wang, S.; Cole, I. S.; Zhao, D.; Li, Q. The dual roles of functional groups in the photoluminescence of graphene quantum dots. *Nanoscale* **2016**, *8*, 7449-7458.
- (26) Feng, J.; Dong, H.; Pang, B.; Shao, F.; Zhang, C.; Yu, L.; Dong, L. Theoretical study on the optical and electronic properties of graphene quantum dots doped with heteroatoms. *Phys. Chem. Phys.* **2018**, *20*, 15244-15252.
- (27) Liu, B.; Aquino, A. J. A.; Nachtigallová, D.; Lischka, H. Doping Capabilities of Fluorine on the UV Absorption and Emission Spectra of Pyrene-Based Graphene Quantum Dots. *J. Phys. Chem. A* **2020**, *124*, 10954-10966.
- (28) Kalaiyarasan, G.; Joseph, J.; Kumar, P. Phosphorus-Doped Carbon Quantum Dots as Fluorometric Probes for Iron Detection. *ACS Omega* **2020**, *5*, 22278-22288.
- (29) Usachov, D.; Vilkov, O.; Grüneis, A.; Haberer, D.; Fedorov, A.; Adamchuk, V. K.; Preobrajenski, A. B.; Dudin, P.; Barinov, A.; Oehzelt, M.; Laubschat, C.; Vyalikh, D. V. Nitrogen-Doped Graphene: Efficient Growth, Structure, and Electronic Properties. *Nano Lett.* **2011**, *11*, 5401-5407.
- (30) Yadav, R.; Dixit, C. K. Synthesis, characterization and prospective applications of nitrogen-doped graphene: A short review. *J. Sci.: Adv. Mater. Devices* **2017**, *2*, 141-149.
- (31) Jalili, S.; Vaziri, R. Study of the electronic properties of Li-intercalated nitrogen doped graphite. *Mol. Phys.* **2011**, *109*, 687-694.
- (32) Wei, Q.; Tong, X.; Zhang, G.; Qiao, J.; Gong, Q.; Sun, S. Nitrogen-Doped Carbon Nanotube and Graphene Materials for Oxygen Reduction Reactions. *Catalysts* **2015**, *5*, 1574-1602.
- (33) Qu, D.; Zheng, M.; Li, J.; Xie, Z.; Sun, Z. Tailoring color emissions from N-doped graphene quantum dots for bioimaging applications. *Light: Sci. Appl.* **2015**, *4*, e364-e364.
- (34) Younis, M. R.; He, G.; Lin, J.; Huang, P. Recent Advances on Graphene Quantum Dots for Bioimaging Applications. *Front. Chem.* **2020**, *8*, 424.

- (35) Zhu, S.; Song, Y.; Wang, J.; Wan, H.; Zhang, Y.; Ning, Y.; Yang, B. Photoluminescence mechanism in graphene quantum dots: Quantum confinement effect and surface/edge state. *Nano Today* **2017**, *13*, 10-14.
- (36) Bacon, M.; Bradley, S. J.; Nann, T. Graphene Quantum Dots. *Part. Part. Syst. Charact.* **2014**, *31*, 415-428.
- (37) Kohn, W.; Sham, L. J. Self-Consistent Equations Including Exchange and Correlation Effects. *Phys. Rev.* **1965**, *140*, A1133-A1138.
- (38) Casida, M. E.; Jamorski, C.; Casida, K. C.; Salahub, D. R. Molecular excitation energies to high-lying bound states from time-dependent density-functional response theory: Characterization and correction of the time-dependent local density approximation ionization threshold. *J. Chem. Phys.* **1998**, *108*, 4439-4449.
- (39) Ernzerhof, M.; Scuseria, G. E. Assessment of the Perdew–Burke–Ernzerhof exchange-correlation functional. *J. Chem. Phys.* **1999**, *110*, 5029-5036.
- (40) Krishnan, R.; Binkley, J. S.; Seeger, R.; Pople, J. A. Self consistent molecular orbital methods. XX. A basis set for correlated wave functions. *J. Chem. Phys.* **1980**, *72*, 650-654.
- (41) Zhao, M.; Yang, F.; Xue, Y.; Xiao, D.; Guo, Y. A Time-Dependent DFT Study of the Absorption and Fluorescence Properties of Graphene Quantum Dots. *ChemPhysChem* **2014**, *15*, 950-957.
- (42) Elgengehi, S. M.; El-Taher, S.; Ibrahim, M. A. A.; Desmarais, J. K.; El-Kelany, K. E. Graphene and graphene oxide as adsorbents for cadmium and lead heavy metals: A theoretical investigation. *Appl. Surf. Sci.* **2020**, *507*, 145038.
- (43) Paier, J.; Marsman, M.; Kresse, G. Why does the B3LYP hybrid functional fail for metals? *J. Chem. Phys.* **2007**, *127*, 024103.
- (44) Qian, Z.; Ma, J.; Shan, X.; Shao, L.; Zhou, J.; Chen, J.; Feng, H. Surface functionalization of graphene quantum dots with small organic molecules from photoluminescence modulation to bioimaging applications: an experimental and theoretical investigation. *RSC Adv.* **2013**, *3*, 14571-14579.
- (45) Ramasubramaniam, A. Electronic structure of oxygen-terminated zigzag graphene nanoribbons: A hybrid density functional theory study. *Phys. Rev. B.* **2010**, *81*, 245413.
- (46) Cossi, M.; Rega, N.; Scalmani, G.; Barone, V. Energies, structures, and electronic properties of molecules in solution with the C-PCM solvation model. *J. Comput. Chem.* **2003**, *24*, 669-681.
- (47) Liu, B.; Gao, Y.; Jabed, M. A.; Kilina, S.; Liu, G.; Sun, W. Lysosome Targeting Bisterpyridine Ruthenium(II) Complexes: Photophysical Properties and In Vitro Photodynamic Therapy. *ACS Applied Bio Materials* **2020**, *3*, 6025-6038.
- (48) Frisch, M. J.; Trucks, G. W.; Schlegel, H. B.; Scuseria, G. E.; Robb, M. A.; Cheeseman, J. R.; Scalmani, G.; Barone, V.; Petersson, G. A.; Nakatsuji, H. et al.: Gaussian 16 Rev. B.01. Wallingford, CT, 2016.
- (49) Humphrey, W.; Dalke, A.; Schulten, K. VMD: Visual molecular dynamics. *J. Mol. Graphics* **1996**, *14*, 33-38.
- (50) Guido, C. A.; Cortona, P.; Mennucci, B.; Adamo, C. On the Metric of Charge Transfer Molecular Excitations: A Simple Chemical Descriptor. *J. Chem. Theory Comput.* **2013**, *9*, 3118-3126.
- (51) Wang, J.; Cao, S.; Ding, Y.; Ma, F.; Lu, W.; Sun, M. Theoretical Investigations of Optical Origins of Fluorescent Graphene Quantum Dots. *Sci. Rep.* **2016**, *6*, 24850.
- (52) Chen, J.-L.; Yan, X.-P.; Meng, K.; Wang, S.-F. Graphene Oxide Based Photoinduced Charge Transfer Label-Free Near-Infrared Fluorescent Biosensor for Dopamine. *Anal. Chem.* **2011**, *83*, 8787-8793.
- (53) Kim, S.; Hwang, S. W.; Kim, M.-K.; Shin, D. Y.; Shin, D. H.; Kim, C. O.; Yang, S. B.; Park, J. H.; Hwang, E.; Choi, S.-H.; Ko, G.; Sim, S.; Sone, C.; Choi, H. J.; Bae, S.; Hong, B. H. Anomalous Behaviors

- of Visible Luminescence from Graphene Quantum Dots: Interplay between Size and Shape. *ACS Nano* **2012**, *6*, 8203-8208.
- (54) Zhao, L.; He, R.; Rim, K. T.; Schiros, T.; Kim, K. S.; Zhou, H.; Gutiérrez, C.; Chockalingam, S. P.; Arguello, C. J.; Pálová, L.; Nordlund, D.; Hybertsen, M. S.; Reichman, D. R.; Heinz, T. F.; Kim, P.; Pinczuk, A.; Flynn, G. W.; Pasupathy, A. N. Visualizing Individual Nitrogen Dopants in Monolayer Graphene. *Science* **2011**, *333*, 999-1003.
- (55) Lherbier, A.; Blase, X.; Niquet, Y.-M.; Triozon, F.; Roche, S. Charge Transport in Chemically Doped 2D Graphene. *Phys. Rev. Lett.* **2008**, *101*, 036808.
- (56) Baimuratov, A. S.; Tepliakov, N. V.; Gun'ko, Y. K.; Baranov, A. V.; Fedorov, A. V.; Rukhlenko, I. D. Mixing of quantum states: A new route to creating optical activity. *Sci. Rep.* **2016**, *6*, 5.
- (57) Lu, T.; Chen, F. Multiwfn: A multifunctional wavefunction analyzer. *J. Comput. Chem.* **2012**, *33*, 580-592.

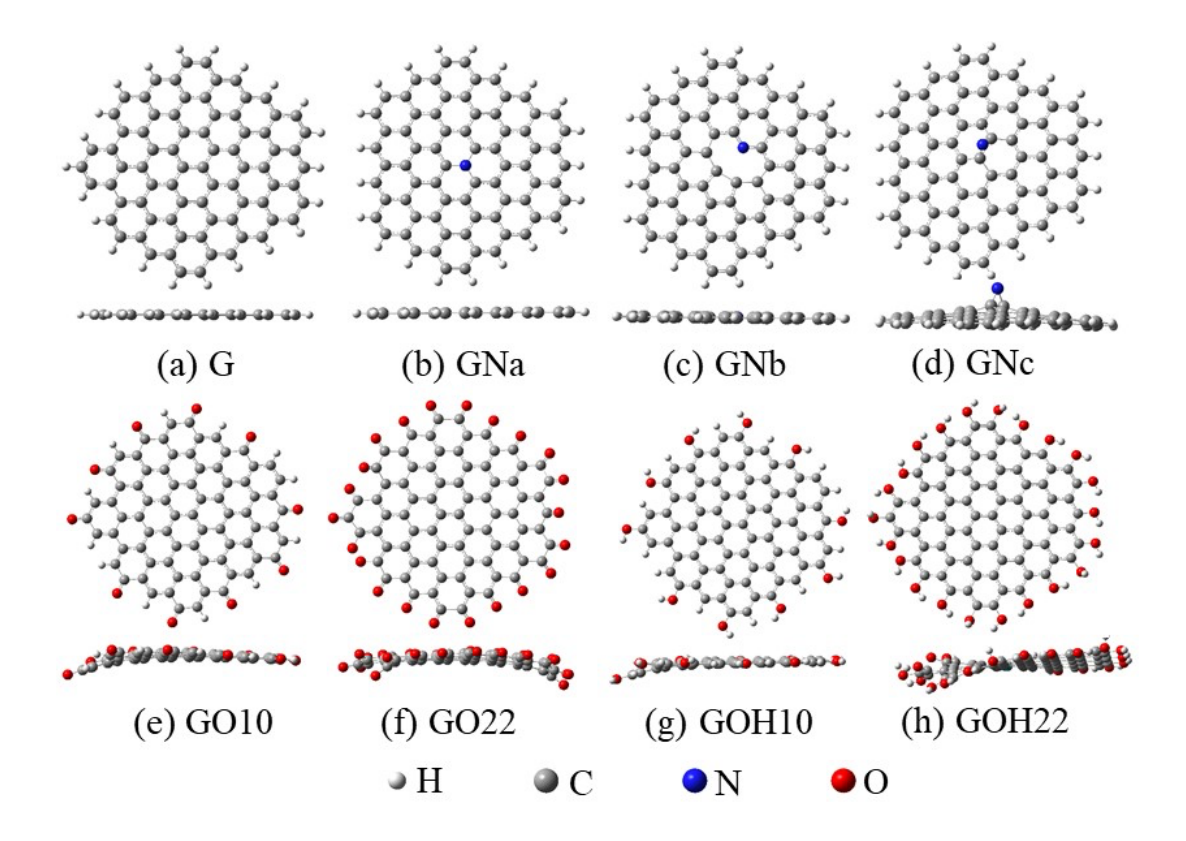
Table 1: The excitation energy, oscillator strength, charge transfer length ( $\Delta r$ ), and C, N, and O atomic orbital contribution in the occupied and unoccupied molecular orbitals for selective excited states of the modeled quantum dots. The excitation energy is in eV, and  $\Delta r$  is in Å unit.

	$S_{\rm n}$	Energy	Oscillato r Strength	Charge transfer length $\Delta r$	МО							
Name					Carbon		Nitrogen		Oxygen			
					Occ	Uocc	Occ	Uocc	Occ	Uoco		
G	S <sub>1</sub>	1.78	0.7515	0.02	1.00	1.00	-	-	-	-		
	<b>S</b> 5	2.49	1.2055	1.73	1.00	1.00	-	-	-	-		
	S <sub>1</sub>	0.27	0.0038	3.09	0.73	0.80	-	-	0.27	0.20		
GO10	$S_2$	0.70	0.1251	4.94	0.80	0.80	-	-	0.20	0.20		
•	<b>S</b> <sub>5</sub>	1.21	0.2046	0.63	0.81	0.78	-	-	0.19	0.22		
	$S_1$	0.18	0.0002	6.53	0.69	0.44	-	-	0.31	0.56		
GO22	S <sub>16</sub>	0.93	0.0720	4.67	0.53	0.56	-	-	0.47	0.44		
	S <sub>38</sub>	1.60	0.6498	3.93	0.66	0.63	-	-	0.34	0.37		
GOH10	$S_1$	1.70	0.7277	0.14	0.92	0.95	-	-	0.08	0.05		
	S <sub>4</sub>	2.21	0.1613	0.80	0.92	0.96	-	-	0.08	0.04		
	<b>S</b> <sub>5</sub>	2.34	1.0603	1.75	0.91	0.95	-	-	0.09	0.05		
GOH22	$S_1$	1.62	0.6580	0.82	0.85	0.87	-	-	0.15	0.13		
	$S_2$	1.75	0.1195	1.70	0.85	0.93	-	-	0.15	0.07		
	<b>S</b> <sub>5</sub>	2.26	0.7739	2.42	0.83	0.88	-	-	0.17	0.12		
GNa	$S_1$	0.76	0.0000	0.00	1.00	0.84	0.00	0.16	-	-		
	S <sub>3</sub>	1.60	0.4467	0.80	1.00	1.00	0.00	0.00	-	-		
	S <sub>6</sub>	2.31	0.2155	0.38	1.00	1.00	0.00	0.00	-	-		
GNb -	$S_1$	0.65	0.0001	0.05	0.94	1.00	0.06	0.00	-	-		
	$S_2$	1.53	0.4153	1.09	1.00	1.00	0.00	0.00	-	-		
	S <sub>3</sub>	1.73	0.4945	1.34	0.98	1.00	0.02	0.00	-	-		
	S <sub>7</sub>	2.36	0.5382	0.36	0.94	0.97	0.06	0.03	-	-		
GNc	$S_1$	0.49	0.0002	1.87	0.62	0.99	0.38	0.01	-	-		
	$S_2$	0.97	0.0643	0.35	0.95	0.99	0.05	0.01	-	-		
	<b>S</b> <sub>5</sub>	1.66	0.4950	1.50	1.00	0.99	0.00	0.01	-	-		
GNaO4	$S_1$	0.40	0.1044	4.10	0.86	0.85	0.00	0.00	0.14	0.15		
	$S_2$	0.90	0.1685	1.99	0.82	0.85	0.02	0.00	0.16	0.15		
	S <sub>4</sub>	1.46	0.2359	3.84	0.85	0.91	0.00	0.01	0.15	0.08		
GNaO6	S <sub>1</sub>	0.74	0.3306	5.35	0.80	0.84	0.01	0.01	0.19	0.15		

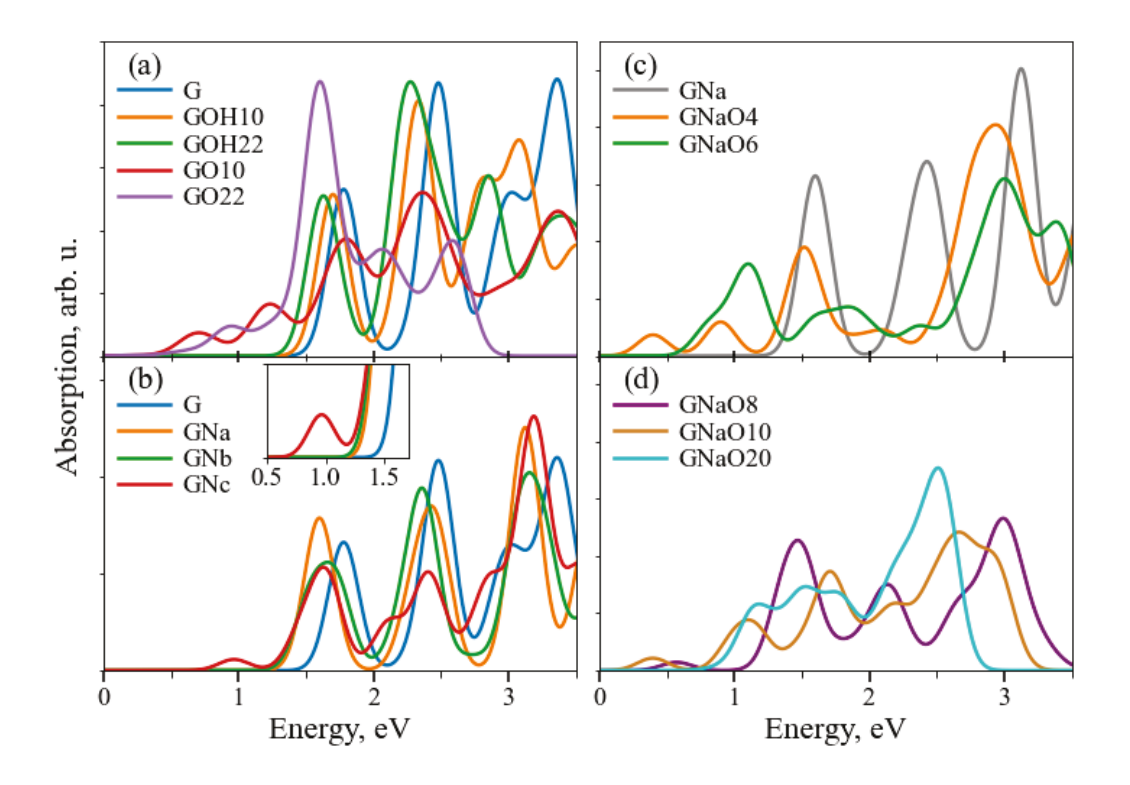
	S3	1.01	0.4792	3.97	0.79	0.84	0.01	0.01	0.20	0.15
-	S4	1.11	0.2499	6.42	0.79	0.82	0.01	0.00	0.20	0.18
	$S_1$	0.57	0.0403	8.02	0.75	0.79	0.01	0.03	0.24	0.18
GNaO8	S <sub>3</sub>	1.36	0.3258	1.76	0.79	0.79	0.01	0.02	0.20	0.18
-	$S_5$	1.53	0.4128	4.12	0.85	0.79	0.00	0.02	0.15	0.19
	$S_1$	0.40	0.0608	6.38	0.77	0.77	0.00	0.00	0.23	0.23
GNaO10	S <sub>3</sub>	1.16	0.1845	3.15	0.77	0.74	0.00	0.04	0.23	0.22
-	$S_7$	1.69	0.2558	2.14	0.82	0.77	0.01	0.01	0.17	0.22
	$S_1$	0.12	0.0001	6.07	0.71	0.45	0.01	0.00	0.28	0.58
GNaO20	$S_8$	1.13	0.1862	4.79	0.64	0.63	0.01	0.00	0.34	0.37
-	S <sub>13</sub>	1.51	0.3121	2.17	0.66	0.66	0.01	0.00	0.34	0.34

Table 2: The X, Y, and Z components of the transition dipole moments (TDM) decomposed on the edge carbons, core carbons, modified oxygens, and doped nitrogen for the  $S_1$  states of the considered quantum dots. The unit is a.u.

	Edge Carbon			Oxygen			Core Carbon			Nitrogen			Total		
Name	X	Y	Z	X	Y	Z	X	Y	Z	X	Y	Z	X	Y	Z
G	-6.50	0.05	0.09	_	-	-	-0.82	-0.12	0.00	_	-	-	-7.32	-0.07	0.09
GO10	0.29	-0.81	-0.69	0.41	-0.10	-0.46	0.30	1.11	-0.54	_	-	-	1.01	0.20	-1.69
GO22	0.24	-0.17	-0.24	1.44	1.40	0.06	-0.71	-1.20	-0.24	_	-	-	0.98	0.03	-0.42
GOH10	5.89	-0.23	0.35	0.81	0.44	0.06	0.64	-0.09	0.00	_	_	-	7.34	0.12	0.42
GOH22	-5.31	-0.21	0.49	-1.84	-0.39	0.12	-0.10	0.71	0.09	_	-	-	-7.24	0.10	0.70
GNa	0.00	0.00	0.00	_	-	_	0.00	0.00	0.00	0.00	0.00	0.00	0.00	0.00	0.00
GNb	0.25	-0.14	0.01	_	_	_	0.04	-0.02	0.00	0.01	0.00	0.00	0.29	-0.17	0.01
GNc	-1.81	-1.93	-0.95	-	-	-	1.86	2.06	1.33	1.98	2.21	1.38	0.06	0.12	0.39
GNaO4	4.49	1.45	-0.33	0.68	-0.02	-0.16	0.98	0.74	0.15	0.02	-0.02	-0.00	6.15	2.17	-0.34
GNaO6	4.67	2.88	0.32	0.97	0.84	0.00	-0.69	-0.83	-0.72	-0.21	-0.22	-0.11	4.95	2.89	-0.40
GNaO8	1.67	-0.01	-0.17	0.04	-1.18	-0.44	2.36	1.45	0.52	0.28	0.30	0.15	4.06	0.25	-0.09
GNaO10	-1.78	-1.38	0.22	-1.16	-0.93	0.03	-0.99	-0.48	0.13	0.00	0.00	0.00	-3.93	-2.80	0.38
GNaO20	-0.04	0.02	0.02	-1.17	-0.90	-0.29	0.61	0.59	0.30	0.00	0.00	0.00	-0.60	-0.29	0.03



**Figure 1:** The optimized geometries of GQD, N-doped GQD, and GQD with edge oxygenous modification. The graphene quantum dot model is G, C<sub>76</sub>H<sub>22</sub> (a). Figures b, c and d are the three different N doping types, name GNa, GNb, and GNc, respectively. The edge modifications with different numbers of the -OH and =O groups include GO10 (e), GO22 (f), GOH10 (g), and GOH22 (h).



**Figure 2**: The calculated absorption spectra of (a): the graphene, graphene oxide (GO10 and GO22) and graphene hydroxide (GOH10 and GOH22) quantum dots; (b): three types of N-doped GQD; and (c) and (d): the GNa type of N-doped GQD with different numbers of edge-modified =O groups. All calculations are performed using the linear response time-dependent DFT with PBE0 functional and 6-31G\* basis set.

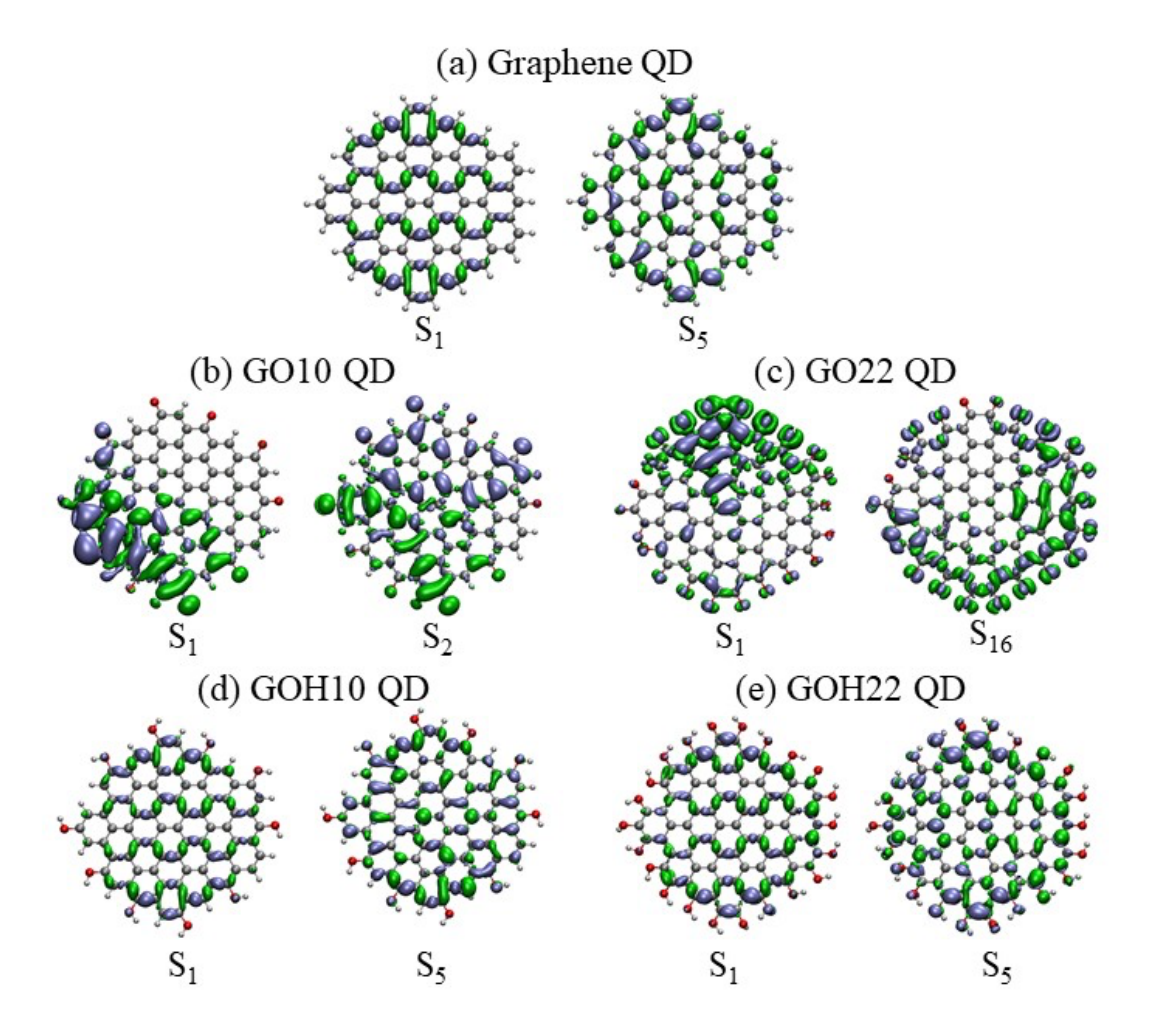


**Figure 3**: The charge density difference maps of selective excited states in the graphene (a), graphene oxide, GO10 (b) and GO22 (c), and graphene hydroxide GOH10 (d) and GOH22 (e) quantum dot. The maps were calculated by subtracting the excited state electron density from the ground state electron density, where Green color represents the positive holes, and dark turquoise represents the negative electrons.

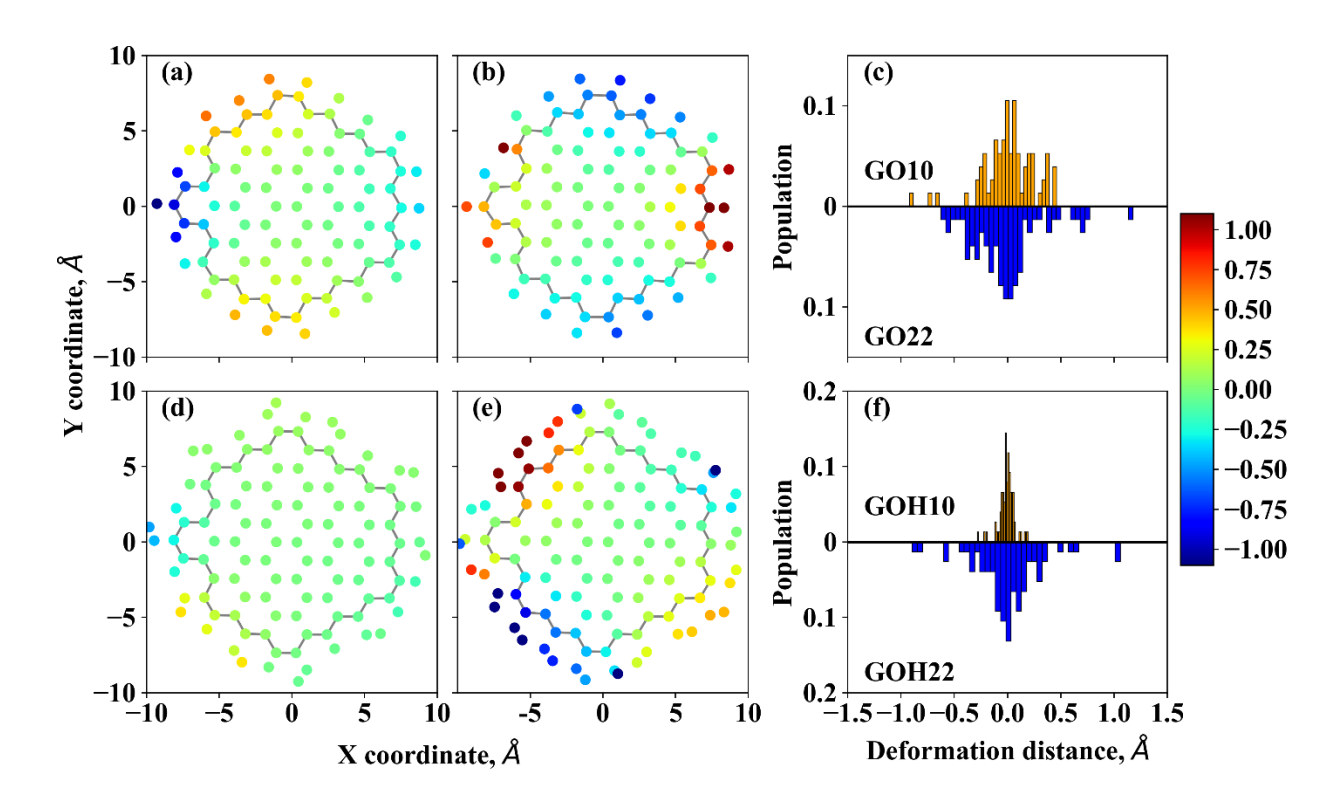


**Figure 4**: The deformation maps of GO10 (a), GO22 (b), GOH10 (d), and GOH22 (e). The color-coded magnitude of the deformation from the graphene plane was mapped onto each atom in the quantum dots. The deformation values were obtained by equation S1. The gray line indicates the edge carbons of the quantum dots. Figures c and f are showing the normalized histograms of the deformation distance distribution.

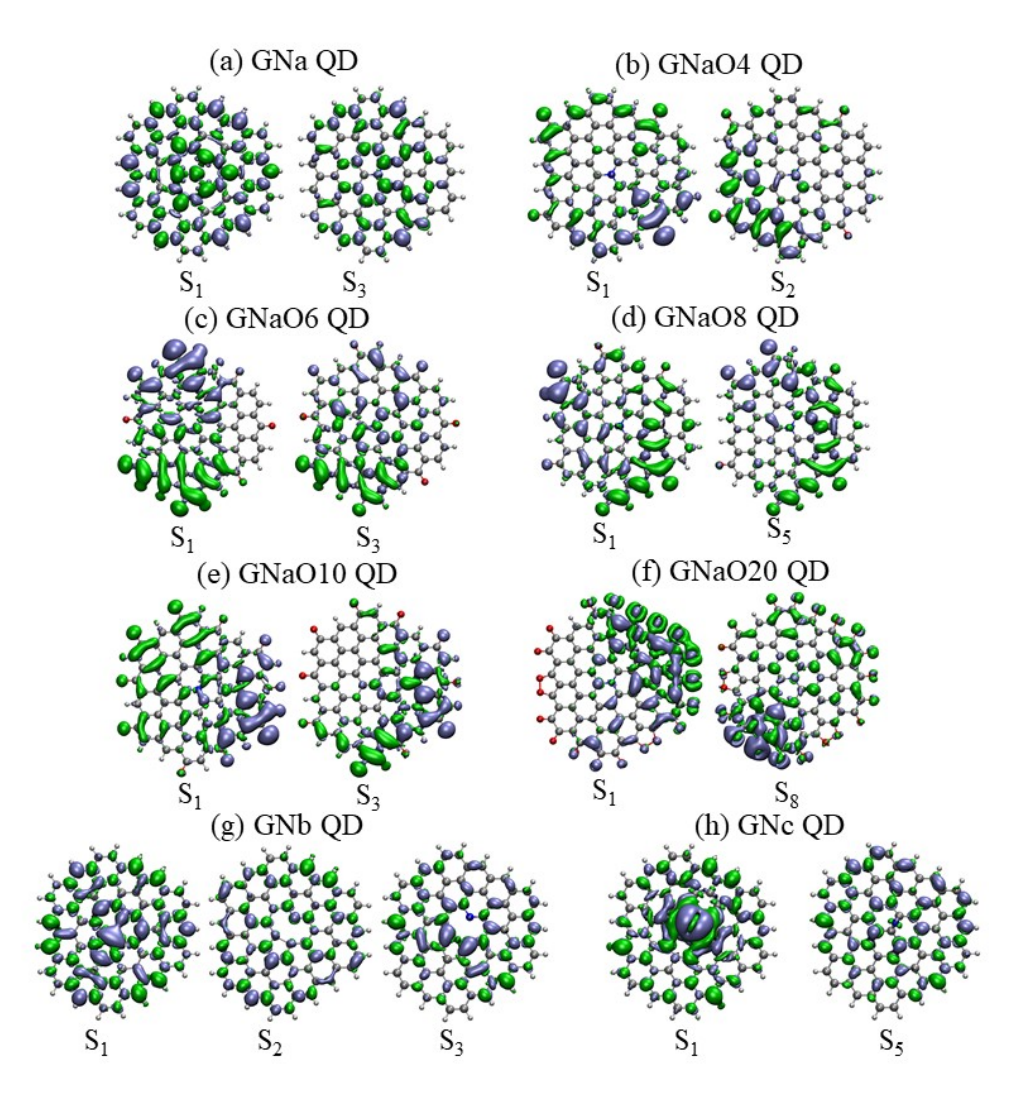


**Figure 5:** The charge density difference maps for the selective excited states in the GNa (a), GNb (g), and GNc (h) quantum dots as well as the oxidized GNa quantum dots with different O/C ratios: GNaO4 (b), GNaO6 (c), GNaO8 (d), GNaO10 (e), and GNaO20 (f). The maps were calculated by subtracting the excited state electron density from the ground state electron density, Green color represents the positive holes and dark turquoise represents the negative electrons.

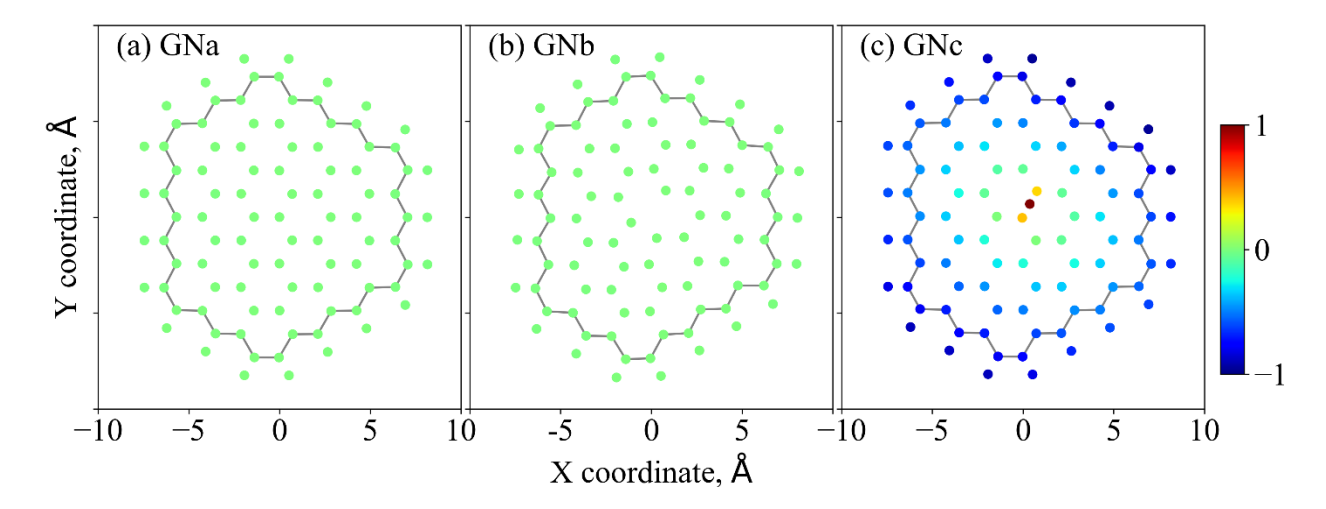


**Figure 6**: The deformation maps of the GNa, GNb, and GNc quantum dots. The color-coded magnitude of the deformation from the graphene plane was mapped onto each atom in the quantum dots. The deformation distance values are obtained by equation S1. The gray line indicates the edge carbons of the quantum dots.

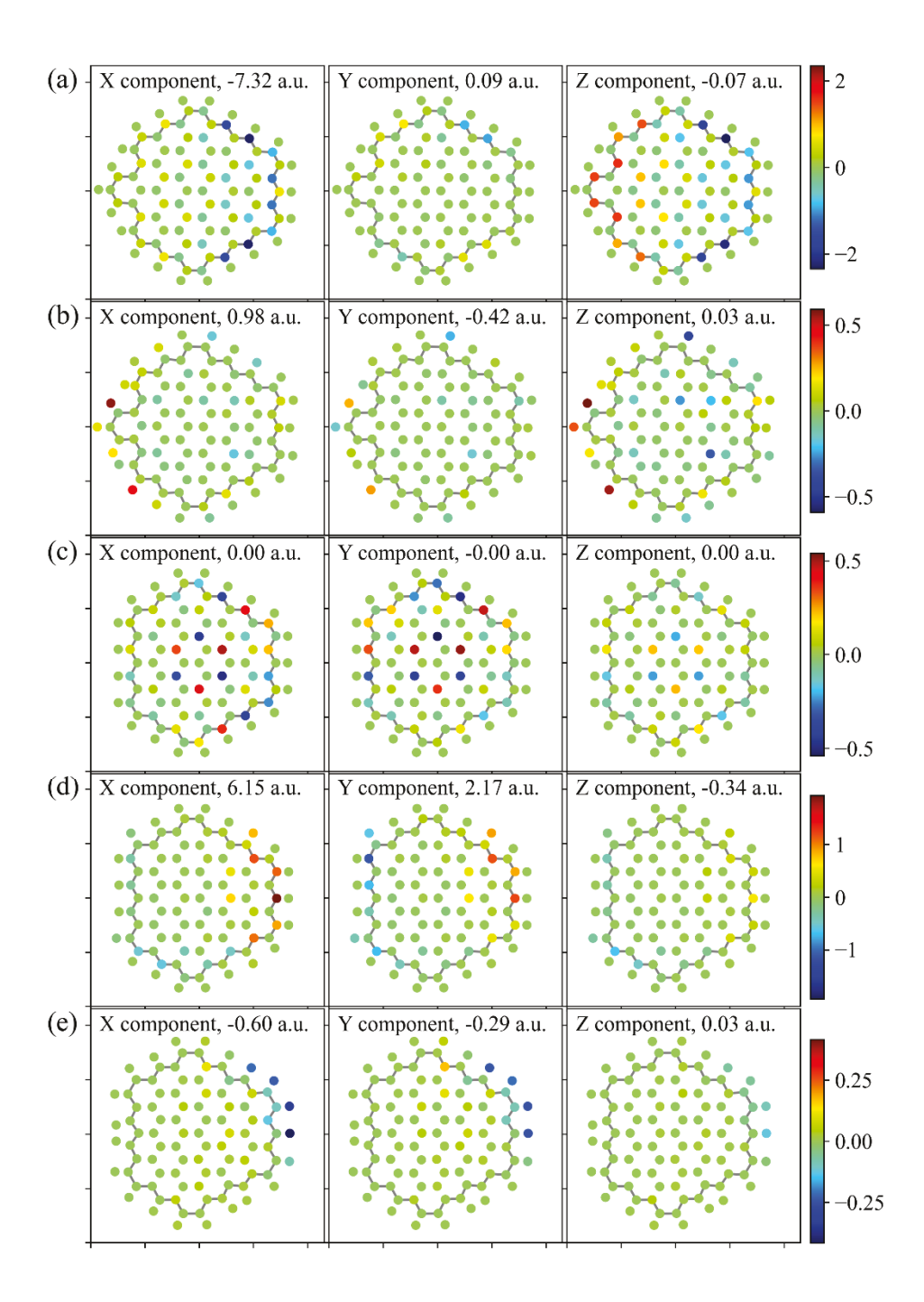


**Figure 7**. The maps of the X-, Y-, Z- component of the transition dipole moment (TDM) of S<sub>1</sub> excitations decompose to atoms of the model G (a), GO22 (b), GNa (c), NGO4 (d), and NGO20 (e). The magnitude is the decomposition of the molecular transition dipole moment on each atom. The gray line indicates the edge carbon of the quantum dots.